

North Atlantic thermohaline circulation predictability in a coupled ocean-atmosphere model

Stephen M. Griffies† and Kirk Bryan‡

Princeton University
Atmospheric and Oceanic Sciences Program
Sayre Hall, Forrestal Campus
Princeton University, Princeton NJ 08544-0710

†email: smg@gfdl.gov

‡email: kbryan@splash.princeton.edu

Submitted to *Journal of Climate*
Los Alamos e-print ao-sci/9502001

Abstract

Predictability of the North Atlantic thermohaline circulation (THC) variability as simulated in the Geophysical Fluid Dynamics Laboratory's coupled ocean-atmosphere general circulation model is established for a set of ensemble experiments. There is a large separation of time scales between the slower oceanic processes, whose predictability is of interest here, and the much more rapid atmospheric processes to which the ocean is coupled. The ensembles consist of identical oceanic initial conditions underneath a model atmosphere chosen randomly from the model climatology. This experimental design is based on the separation in time scales present in the model which motivates the assumption that the predictability deduced from these ensembles provides an upper limit to the model's THC predictability. The climatology, against which the ensemble statistics are compared, is taken from a multi-century model integration whose THC variability has power concentrated at the 40-60 year time scale. A linear stochastic perspective, motivated from Brownian motion and THC box model case studies, is shown to be generally consistent with the ensemble statistics. The linear theory suggests a natural measure of ensemble predictability as the time at which the ensemble variance becomes a subjectively defined fraction (50% used here) of the climatological variance. It is furthermore of interest to distinguish predictability of the rapidly de-correlating portion of the model's THC from the longer time correlated portion. The rapidly de-correlating portion shows predictability for ≈ 1.5 years. The slower portion shows predictability for $\approx 5 - 7$ years. The linear stochastic framework provides for the straightforward construction of an optimal forecast of the model's THC variability. It also allows for an understanding of why the optimal forecast is useless beyond a particular predictability limit.

1 Introduction

1.1 North Atlantic variability

Recent analysis of historical data by Levitus (1989a,1989b,1990), Deser and Blackmon (1993), and Kushnir (1994) indicate the existence of a significant amount of interannual to interdecadal variability in the North Atlantic climate system. The correlation between North Atlantic climate variability and that of adjacent land regions is of interest in part because of the desire to forecast that variability most affecting human populations. At present, there is insufficient observational and proxy evidence to clearly indicate the significance of the correlations seen in the data record. For example, the analysis by Broecker et al. (1985) of the large climatic fluctuation from the warm Alleröd to glacial Younger Dryas periods (approximately 11,000 years ago) suggests that North Atlantic variability at that time was correlated to only certain regions of western Eurasia and coastal regions of northeast North America into Greenland. The recent analysis by Schlesinger and Ramankutty (1994) of the last 100 years of global surface air temperatures, however, suggests a stronger and more coherent relationship between the North Atlantic variability during this recent period and that of adjacent land regions. Yet it cannot be determined whether this behavior is typical until longer time series of proxy data from different parts of the globe become available.

A primary objective of several climate research programs, such as the Atlantic Climate Change Program (ACCP), the Atlantic portion of the World Ocean Circulation Experiment (WOCE), and the second phase of the Climate Variability and Prediction Research Programme (CLIVAR), is to design practical programs for monitoring climate variability of decadal and multidecadal time scales such as that having been observed in the North Atlantic. The monitoring would be focused on natural climate variations and the detection of possible long term anthropogenic climate change. Presently, it is not clear what the requirements for such a monitoring system are. One motivation for the present study is to initiate studies useful for assessing the utility of such an observing system for the prediction of natural climate variability in the North Atlantic. Furthermore, the extent to which North Atlantic variability is correlated to that of surrounding land regions may indicate the extent to which the monitoring of such variability aids in forecasting climate variability of relevance to human populations. Presently, the TOGA TAO (Tropical Ocean and Global Atmosphere / Tropical Atmosphere Ocean) array, in conjunction with other measurements made from satellites and ships of opportunity, provides input which appears to allow a useful basis for coupled ocean-atmosphere model projections of El Niño – Southern Oscillation (ENSO) (e.g., Neelin et al. 1994). One question is whether the very different air-sea interaction processes involved in North Atlantic climate variability can likewise be projected forward in time using coupled ocean-atmosphere models, but allowing for the added involvement of the deep ocean in which the thermohaline circulation (THC) plays an

important role.

The THC is a major component of the ocean circulation and is particularly important for poleward heat transport by ocean currents to high latitudes in the North Atlantic. This role of the ocean's THC in affecting long term North Atlantic variability was suggested by Bjerknes (1964) (see Bryan and Stouffer 1991 for a survey). Therefore, assuming a close link between low frequency North Atlantic climate variability and THC variability, the physical basis of North Atlantic climate predictability is related to predictability of the THC. It is with this connection in mind that the current coupled ocean-atmosphere model predictability study is undertaken with focus on the model's THC variability.

1.2 Modeling the thermohaline circulation

Since the THC is thought to be especially important for North Atlantic climate, numerous modeling efforts have focused on understanding the stability and variability of the THC. In regards to stability, Stommel's two box model (1961) highlighted the importance of the different oceanic boundary forcing contributed by heat and hydrology. In this model, more than one stable mode of circulation is available: one with the thermally dominant circulation corresponding to that acting in today's climate and another with a reversed flow dominated by haline effects. F. Bryan (1986) initiated a continuing effort to establish the stability of a hierarchy of ocean-only models forced under mixed boundary conditions (linear damping of sea surface temperature (SST) to a specified value and constant hydrological fluxes affecting sea surface salinity (SSS)). In a general circulation model (GCM) simulation, he was able to create a shut down of the THC after placing an anomaly of fresh water in the northern portion of the model. Further studies of ocean-only models using mixed boundary conditions exhibit a wide range of stability and variability properties depending on the strength of the forcing used (see Weaver and Hughes 1992 for a survey).

Ocean-only climate models can be considered crude approximations to the more physically complete coupled ocean-atmosphere models since the surface boundary conditions in the ocean-only models are intended to emulate coupling to an atmosphere. Furthermore, as the THC is driven by surface buoyancy fluxes embodied in the model's boundary conditions, the behaviour of the THC in ocean-only models can vary widely depending on the strength of the forcing and the feedbacks incorporated. Recently, some groups have begun to reexamine the suitability of some mixed boundary condition models as an approximation to the ocean-atmosphere coupling. For example, Zhang et al. (1993) and Mikolajewicz and Maier-Reimer (1994) have suggested the relevance of particular modifications to their model's heat transport feedbacks, as parametrized by surface temperature restoring times, in such a manner which yields a more stable model behaviour. Rahmstorf (1994) presents the results of a model forced with fixed hydrological fluxes yet with a modified temperature boundary condition acting in a scale dependent manner. This model appears to be more stable to an overall

collapse of the THC under hydrological perturbations although it is quite unstable to changes in the particular convection pattern relevant for the model's THC. In addition to questioning the form of the temperature feedbacks acting in the models, Tziperman et al. (1994) have questioned the use of strong hydrological forcing which, under the usual mixed boundary conditions, can result in highly variable and unstable model THC simulations. It is suggested that a more reasonable magnitude of hydrological forcing results in a more stable mixed boundary condition model.

In addition to formulating the deterministic boundary conditions parametrizing the ocean-atmosphere interactions, understanding the effects of atmospheric fluctuations acting on the ocean's surface can be important for modeling the ocean's variability. To date, these fluctuations in ocean-only models have taken the form of a stochastic forcing such as that used by the Max Planck Institute in Hamburg (e.g., Hasselmann 1982, Mikolajewicz and Maier-Reimer 1990, Weisse et al. 1994). As discussed in the next subsection, we believe that a stochastic perspective is appropriate for interpreting the coupled model THC ensemble experiments reported in this paper. It should be noted that the precise form of a prescribed stochastic forcing (i.e., the spatial and temporal correlations, power of the stochastic forcing, and feedbacks) acting on an ocean-only model inevitably plays a large part in determining the model's response. Finding appropriate forms of this non-deterministic forcing, which conceivably requires the use of fully coupled ocean-atmosphere models as well as observational data, is arguably at least as difficult a problem as determining appropriate deterministic boundary conditions.

An alternative to highly parameterized representations of an atmosphere coupled to a more detailed ocean circulation model is to couple a more explicit numerical model of the atmosphere to an ocean model. Such models do not rely on the approximations to air-sea interactions necessary for setting upper ocean boundary conditions in ocean-only models. Nor do they assume *a priori* a particular statistical character of the atmospheric component. Yet these models have their problems as well. Firstly, they are quite expensive to run. For example, the coupled model used in the present study requires 1.5–2.0 Cray-YMP hours per model year. This expense greatly constrains the statistics available from the coupled model ensemble experiments reported here. It furthermore motivates the study of simpler models in combination with the more realistic models. Secondly, fully coupled models require adjustments of the ocean-atmospheric fluxes (Manabe and Stouffer 1988, Sausen et al. 1988) in order to prevent a drift of the model's mean state away from geophysically relevant regimes. The working hypothesis employed in the flux adjusted models is that such adjustments, as they have no variability on the time scales of interest, will not unrealistically affect the model's long term variability. There is no rigorous proof of this hypothesis other than direct validation of the model output with the observational data record. The physical relevance of studies using models with unrealistic mean states, which result from the non-flux-adjusted coupled models used to date, is unclear. From our perspective, sufficiently validated flux adjusted coupled GCMs are the best available tool for addressing North Atlantic climate variability issues, including its predictability.

An example of a flux adjusted coupled model which exhibits climate variability consistent with certain North Atlantic observations is that of Delworth et al. (1993; henceforth DMS93) who used the Geophysical Fluid Dynamics Laboratory's (GFDL) coupled global ocean-atmosphere GCM. This model presents a realistic simulation of the air-sea interaction over the Atlantic basin on the yearly to interdecadal time scales and produces a low frequency variability qualitatively similar to that seen in the analysis of Levitus (1989a) and Kushnir (1994). Since the low frequency variability in the model's North Atlantic is associated with THC fluctuations, the model successfully embodies Bjerknes' hypothesis for North Atlantic variability. As can be seen in the model analysis of Manabe and Stouffer (1988), which discuss the model's behaviour when the North Atlantic THC is both active and shut down, the correlation between the model's North Atlantic SST variability and adjacent surface temperature over land masses suggests a distinct downstream influence in the direction of atmospheric flow as found by Broecker et al. (1985) from paleoclimate data. On the other hand, Schlesinger and Ramankutty (1994) show that the single 50–60 year swing in climate which shows up in historical records indicates an association of SST in the North Atlantic with both upstream and downstream surface temperature over the adjacent land areas.

Given the compelling model and observational evidence for low frequency variability of the North Atlantic, as well as the important role played by the ocean's THC, understanding the predictability of model simulated THC is a necessary step towards assessing the possibilities of producing long term North Atlantic climate forecasts. It is for this reason that a study of the North Atlantic THC predictability using the GFDL coupled ocean-atmosphere model has been undertaken.

1.3 A stochastic perspective

Climate systems, through the presence of various coupled sub-systems, typically contain a broad range of space and time scales which can be defined by representative auto-correlation scales. In the context of the coupled ocean-atmosphere system relevant for this study, time scales range roughly from the short time scale synoptic atmospheric processes (on the order of days) to the long time scale oceanic processes (on the order of years and longer). It is the response of the ocean on longer time and larger space scales through processes associated with the THC that are of interest in the current study.

Atmospheric model and observational studies indicate a loss of deterministic predictability of typical mid-latitude synoptic scale motions at the 10 day time scale (see Lorenz 1969 for an early review of atmospheric predictability). At times longer than the synoptic predictability time the atmosphere is effectively non-deterministic. The recent work by Kleeman and Power (1994) and Power et al. (1995) have pointed towards the importance of this random variability in affecting the predictability of the coupled ocean-atmosphere system. Nevertheless, the hope is that by exploiting

the memory of the slower time scale processes, namely the ocean circulation, useful long term predictions of the coupled system are possible. For example, it is this oceanic memory which allows for better than climatology ENSO forecasts up to a year in advance (e.g., Neelin et al. 1994). Given that the variability in the North Atlantic circulation affects the long term atmospheric statistics in this region, it is necessary, although not sufficient, to characterize the predictability limits of the oceanic sub-system in order to assess the feasibility of forecasting low frequency climate statistics.

Hasselmann (1976), through exploiting the time scale separation between various portions of the climate system, demonstrated the relevance of linear stochastic climate models for understanding the red noise response of certain climate processes, such as SST, to white noise forcing which can approximate that provided by rapidly de-correlating portions of the system, such as synoptic atmospheric variability. Subsequent modeling efforts have supported and extended Hasselmann's perspective. For example, Mikolajewicz and Maier-Reimer (1990) and Weisse et al. (1994) forced the Hamburg large scale geostrophic ocean model (Hasselmann 1982) with spatially correlated white noise fresh water fluxes. These studies identified linear oceanic modes of variability in the model's Atlantic basin. A similar study was carried out by Mysak et al. (1993) using a two dimensional THC model with random hydrological fluxes. This study also resulted in the excitation of various oceanic modes. From a more idealized perspective, Bryan and Hansen (1994) considered the variability of the Stommel (1961) two-box model when forced with white noise buoyancy fluxes. Their motivation was to extend Hasselmann's SST model to include salinity effects in the process of producing a toy model description of the variability seen in DMS93. As an extension of Bryan and Hansen, the study by Griffies and Tziperman (1995; hereafter GT95) show how random heating of a mixed boundary condition four-box model emulates the variability and temperature–salinity–THC phase relations seen in the coupled model simulation of DMS93. The excitation of a linear damped oscillatory THC mode dominates the variability in their four-box model.

1.4 The present ensemble predictability study

Predictability studies are concerned with the feasibility of making predictions for dynamical systems on the basis of incomplete or "imperfect" initial conditions. Expressed in another way, predictability is concerned with the length of time for which a prediction can be carried out before errors in the initial conditions rise to the values of normal variability. From a modeling perspective, predictability studies are a first step towards assessing the possibilities of using the model to forecast the variability of a particular phenomenon. In the early stages of such studies, such as the present, validation of the forecast against reality is not considered. Rather, a characterization of the model's precision is useful in order to determine the significance of a potential forecast. A tool for addressing the precision question is the ensemble experiment in which the model is integrated a number of times starting from

slightly different initial conditions. This method is widely used in atmospheric model predictability studies (e.g., Lorenz 1969). The model is exhibiting predictable behaviour at a particular time if the ensemble statistics are distinguishable, to within a subjective statistical criteria, from the statistics of a climatology. For linear Gaussian processes, which form the basis of the analysis in this paper, a complete comparison of the ensemble and climatology statistics is provided by comparison of their mean and variance. (The recent work of Anderson and Stern 1995 and references therein provide additional discussion of these points.)

This paper considers predictability of the yearly averaged and 10 year low pass yearly averaged amplitude of the THC simulated in the GFDL coupled ocean-atmosphere GCM. Comparison of the statistics from a series of ensemble experiments and a multi-century integration provide a characterization of the ensemble's predictability. In the coupled model context, ensemble predictability studies have also been carried out mostly with ENSO being the phenomenon of interest (e.g., Goswami and Shukla 1991). The authors are unaware of similar studies being conducted with focus on the North Atlantic THC.

A generic perturbation of the atmosphere typically translates within a few days into a completely different atmosphere within the climatology. This behaviour motivates our taking the working hypothesis that the predictability of long term oceanic variability is not significantly affected by the precise initial condition of the atmosphere. Therefore, we consider here coupled model ensembles in which the initial conditions for the atmosphere are taken randomly from model climatology whereas the ocean's initial state is unchanged. Based on the separation in time scales between the atmosphere and oceanic variability considered here, THC predictability deduced from these ensembles should serve as an upper limit to the model's THC predictability. Although the initial condition of the real ocean can never be perfectly known, which implies that ensembles whose elements have different oceanic initial conditions will be necessary to more completely characterize the model's THC predictability, the predictability time scales established here will serve as a useful benchmark to which more realistic studies can be compared.

The remainder of this paper consists of the following sections. Section 2 summarizes the salient features of the coupled model and its variability. Thereafter, a description of the ensemble experiments is presented. Before analyzing the ensemble statistics, we analyze ensemble experiments from a hierarchy of simpler models building on a linear stochastic perspective. For this purpose, Section 3 gives a discussion of ensemble experiments generated by two low order linear stochastic models; namely, the Brownian (or red noise) and harmonic Brownian processes. Section 4 shows how the linear stochastic analysis is useful for understanding the statistics from the THC four-box model of GT95. The presentation given in these two sections attempts to establish a framework providing a concise description of the coupled model ensemble statistics. Furthermore, as we are limited to rather small ensemble sizes with the coupled model due to their expense, the ensembles from the low order

models will be presented with comparable sizes in order gain a sense of the extent to which sampling errors are an issue. Conclusions from these case studies have been verified by ensembles many times larger. The lessons learned from the low order models are applied in Section 5 to the coupled model ensembles. Section 6 presents a discussion of the results and conclusions. Appendix A supplements Section 3 by providing formulae for the stationary statistics of the two Brownian processes.

2 The coupled model ensemble experiments

2.1 The model

The coupled ocean-atmosphere model used here is that of the GFDL and has been employed extensively for global warming research. We use the same configuration as DMS93, in which the North Atlantic variability was analyzed from a multi-century model integration. Reference should also be made to Stouffer et al. (1989) for information regarding the model structure and performance as well as Manabe and Stouffer (1988, 1995), Manabe et al. (1991,1992), and Stouffer et al. (1994) and for added details and analysis.

Briefly, the model's atmospheric component is an R15 spectral model in the horizontal with 9 vertical levels. The ocean component is a global 12 level Bryan-Cox-Semter model with 3.75° longitude by 4.5° latitude resolution. Ocean mixing occurs with an isopycnal scheme described by Tziperman and Bryan (1993) in addition to horizontal and vertical background eddy diffusion on top of a vertical convective adjustment. The model contains the seasonal cycle and employs monthly and geographically dependent adjustments of the heat and fresh water fluxes (Manabe and Stouffer, 1988).

2.2 The model THC variability

Figure 1 shows 400 years of linearly detrended (i.e., a least squares fit of a line to the time series has been subtracted) anomalous yearly averaged THC index from the central part of a 1000 year coupled model experiment (provided by Ron Stouffer; see DMS93 and Manabe and Stouffer 1995 for analyses of this model integration). It is this portion of the millennium which serves as a climatology for the subsequent ensemble experiments. The THC index is defined as the maximum value for the North Atlantic meridional circulation streamfunction within the latitudes $40.5^\circ N$ to $72^\circ N$. It is a useful index for measuring the strength of the THC in the North Atlantic region of the model. Furthermore, it is a spatially integrated quantity that is useful for capturing the low frequency variability of the model ocean, which is also associated with low frequency model atmospheric variability (DMS93). To further highlight the low frequency variability, a 10 year low pass filtered version of the time series

is indicated.

For the purposes of conducting a predictability study, a stationary climatology whose variability corresponds to that seen in the ensemble experiments is necessary to quantify the ensemble's predictability. We have chosen the 400 years shown in Figure 1 based on this requirement and the added desire to have a simple linear detrend produce stationarity.

Figure 2 shows the auto-correlation function (*acf*) of the time series in Figure 1. Fit (using a least squares criterion) to the *acf* are the *acfs* from the Brownian or red noise process (fit to lags ≤ 10 years) and that from a noise driven damped harmonic oscillator, also known as the harmonic Brownian process (fit to lags ≥ 10 years). These linear stochastic processes are the continuous versions of first and second order auto-regressive processes, respectively (Jenkins and Watts, 1968) and will be described further in Section 3 and Appendix A. The Brownian process captures the small time lag de-correlation of the THC index whereas the harmonic Brownian process captures the negative trough suggesting a damped oscillatory component in the THC. Similar fits result from using slightly different lag regions.

The above fit was also done to the *acf* from the low pass filtered signal (not shown) and the time scales are given in the caption to Figure 2. As described by Munk (1960), filtering increases the auto-correlation of a damped process, such as the Brownian process, since it filters out part of the rapidly de-correlating portion of the process. Hence, the correlation e-folding times are larger for the filtered process.

It should be noted that the statistical significance of the negative trough in the *acf* of Figure 2 is marginal at the 95% confidence level. Analysis of different portions of the climatology (DMS93 and GT95), as well as certain fields [e.g., dynamic topography (not shown)], nevertheless motivates us to consider the climatology to have a highly damped low frequency oscillatory component coupled to purely damped components, rather than being the result of completely damped processes. This interpretation, which is perhaps a minimal description of the coupled model's THC variability, is also motivated by the box model study of GT95 and discussed in Section 4. The spectral analysis of DMS93 indicate that most of the THC power is broadly spread about the 40-60 year time range. This breadth corresponds to the broad trough in the *acfs* relative to that of the single damped harmonic oscillator fit in Figure 2.

2.3 The ensemble experiments

Two sets of ensemble experiments are reported in this paper and are shown in Figures 3 and 4. The elements of the first ensemble was started from year 130 of the climate run and the second ensemble was started at year 500. Both ensembles extend for 30 years and both started with an initial anomalous circulation greater than one standard deviation from the mean.

The stochastic nature of these time series suggests the hypothesis that the model's THC variability is associated with the effectively random forcing from the model's atmosphere. This idea was suggested in the discussion of DMS93, studied in a box model context by Bryan and Hansen (1993) and GT95, and will be pursued further in the following sections.

3 Predictability in linear noise driven systems

In this section, we discuss two linear, single variable, stochastic models in which a complete statistical description is available from concise and explicit mathematical formulae. Analysis of the predictability of these models' variability will be useful for establishing the basics of ensemble predictability experiments. Furthermore, this analysis will prove to be a relevant general framework for understanding the statistics from the coupled model ensemble experiments.

3.1 The Brownian process

As our first example of linear noise driven processes, consider the *red noise* or *Brownian process* $v(t)$ described by the equation

$$\dot{v}(t) = -\alpha v(t) + \xi(t), \quad (1)$$

where the overdot indicates a time derivative. The parameter $\alpha \geq 0$ represents the effects of frictional forces which are dissipative and act to relax $v(t)$ back to its equilibrium value $v_{eq}(t) = 0$; i.e., it provides a linear negative feedback. $\xi(t)$ represents the rapidly de-correlating forces. This is a fluctuation term which will be modeled as a Gaussian white noise process with zero mean and auto-covariance $\langle \xi(t)\xi(s) \rangle = \sigma_\xi^2 \delta(t-s)$, with $\delta(t)$ the Dirac delta function and σ_ξ^2 determining the power of the noise. The expectation operator $\langle \bullet \rangle$ represents an average over an infinite sized ensemble. As the stochastic processes considered in this paper are linear Gaussian, the first moment stationary statistics from a finite sized ensemble will approximate the statistics of the infinite sized ensemble with correction terms proportional to $N^{-1/2}$, where N is the ensemble size.

In the context of Brownian motion, $v(t)$ represents the velocity $\dot{x}(t)$ of the Brownian particle (see e.g., Reif 1965). Hasselmann (1976) introduced this process into the climate literature as a means of describing the integrative response of a slow climate sub-system, such as the ocean, to a shorter time scale forcing, such as that provided by the synoptic scale atmosphere. We will generically refer to this equation as that describing a *Brownian process*. It is this process which will be argued to be useful for understanding the behaviour of the relatively short time scale portion of the coupled model THC variability. Some details regarding the stationary statistics of this process are given in Appendix A.

3.1.1 The optimal forecast

Although the Brownian process is stochastic and hence non-deterministic, it might still be of interest to produce an optimal forecast of a future state. For this purpose, given observations of a particular realization $v(t)$ over some time ending at $t = 0$, it is useful to ask what is the most probable future state at times $t = \tau > 0$? As discussed recently by Penland (1989) in the meteorological context, since the process is Gaussian, the most probable future state of the system is also that state which is optimal in a least squares sense. For the Brownian process, this state defines the *damped persistence* forecast (see Lorentz 1973 for the discrete case)

$$v_{dp}(\tau) = v(0) \exp(-\alpha\tau); \quad (2)$$

i.e., this forecast is a damping of a persistence forecast $v_{persist}(\tau) = v(0)$ back to a zero anomaly with a relaxation time given by the system's auto-correlation time. It is useful to note that this forecast is the same as the mean of an infinite sized ensemble each of whose elements starts at the initial state $v(0)$.

Since each ensemble element starts from the initial state $v(0)$, a formal expression for a particular ensemble element can be written

$$v(\tau) = v(0)e^{-\alpha\tau} + \int_0^\tau e^{-\alpha(\tau-u)}\xi(u)du \equiv v_{dp}(\tau) + \int_0^\tau e^{-\alpha(\tau-u)}\xi(u)du, \quad (3)$$

where the white noise process $\xi(u)$ differs for each element and the damped persistence forecast (2) was identified. Hence, the mean square difference between the forecast $v_{dp}(\tau)$ and an infinite number of realizations of the process, each of which starts at $v(0)$, provides a natural definition of the error in the forecast:

$$\sigma_{dp}^2(\tau) \equiv \langle (v(\tau) - v_{dp}(\tau))^2 \rangle = \langle v^2 \rangle (1 - e^{-2\alpha\tau}), \quad (4)$$

where $\langle v^2 \rangle = \sigma_\xi^2/2\alpha$ is the climatological or stationary variance of the process (see Appendix A). The error is also understood as the variance in the infinite sized ensemble about its mean state as well as the covariance between the forecast and an infinite number of realizations (again, each of which starts at $v(0)$). It is this measure of the forecast error, and its approximation from finite ensembles, which is appropriate for measuring the predictability remaining in an ensemble forecast of linear Gaussian noise driven systems.

The squared forecast error σ_{dp}^2 approaches the climatological variance with an e-folding time $1/(2\alpha)$. The larger the feedback coefficient α of the Brownian process, the faster the forecast error saturates to that defined by the climatology. Note that this e-folding time for the saturation of the forecast error is one-half the auto-correlation e-folding time for the process. The same error calculation for the persistence forecast $v_{persist} = v(0)$ yields the mean squared error

$$\sigma_{persist}^2(\tau) = \langle (v(\tau) - v(0))^2 \rangle = 2 \langle v^2 \rangle (1 - e^{-\alpha\tau}), \quad (5)$$

which saturates to twice the climatological variance yet at a slower rate than the optimal forecast. The error in the persistence forecast is always larger than that of damped persistence. The slope of the optimal forecast error is given by

$$\frac{d\sigma_{dp}^2}{dt} = 2\alpha\langle v^2 \rangle e^{-2\alpha t}, \quad (6)$$

which indicates an exponentially decaying but positive slope starting at $2\alpha\langle v^2 \rangle$. Filtering a Brownian process will reduce this initial slope, as expected from there being an increase in persistence for filtered signals (Munk 1960).

Some numbers corresponding to the coupled model THC index auto-correlation time scales (Figure 2) are illustrative. With a subjectively defined level of forecast skill $\gamma \equiv \sigma_{dp}^2 / \sigma_{climate}^2 = [1 - \exp(-2\alpha\tau_\gamma)]$, the time τ_γ beyond which the optimal forecast is of no use, which serves to define a *predictability time*, is given by $2\alpha\tau_\gamma = -\ln(1 - \gamma)$. For example, with $\gamma = .5$, $1/\alpha = 5$ years, $\tau_\gamma = 1/(2\alpha) \ln 2 = 1.7$ years. For the less stringent level $\gamma = .75$, the useful lead time is $\tau_\gamma = 3.5$ years. The equivalent calculation for the persistence forecast, whose error is given by equation (5), yields $\alpha\tau_\gamma = -\ln(1 - \gamma/2)$, or a .5 error crossing time of 1.4 years and a .75 error crossing time of 2.4 years.

3.1.2 A numerical example

A finite set of ensemble elements may exhibit either slower or faster saturation of ensemble variance than that described above (to within the constraints set by the sampling errors proportional to $N^{-1/2}$, where N is the ensemble size). Furthermore, as seen in the experiments of this and the following sections, the finite ensemble results most closely approximate the infinite ensemble results at small lead times. The agreement between the finite ensemble results and the infinite results will also depend on the level of the noise in the system, with a higher noise level resulting in more variance about the infinite ensemble results. These points are illustrated in Figures 5 and 6. Figure 5A shows a 200 year realization of the Brownian process. The parameters used for realizing this signal are indicated in the caption. The *acf* for 400 years of the process is shown in Figure 5B. Figure 6A shows a nine element ensemble. The noise forcing is identical for all the elements up to year 65 and differs thereafter. The ensemble mean is shown in Figure 6B. The smoother dashed line is the mean of the infinite sized ensemble; i.e., the damped persistence forecast given by equation (2). Figure 6C shows the ensemble variance. The smoother dashed line is the expected variance (4) from the infinite sized ensemble; i.e., the optimal forecast error. Note that we follow the discussion of Penland (1989) for numerically realizing the stochastic processes considered in this paper (see Kloeden and Platen 1992 for a mathematical treatment).

The above results form the basis of optimally forecasting a red noise or Brownian process. Once an estimation of the system's initial state $v(0)$ (from observations) and auto-correlation time α^{-1}

(from the climatology) has been made, the damped persistence forecast (2), which exponentially damps an anomaly back to zero, is available. This forecast is the best forecast possible in the least squares sense for the red noise process and it is also the most probable future state of the process. The only means for making a useful prediction is afforded by the system's memory. The effectiveness of the damped persistence forecast, as measured by its predictability or ensemble variance e-folding time, is directly related to the system's correlation time.

3.2 The harmonic Brownian process

This section presents the analogous calculations of the previous section for the damped harmonic oscillator driven by Gaussian white noise. This process will be referred to here as the *harmonic Brownian process*. It is this process which will be argued to be useful for understanding the coupled model's THC low frequency variability. The equation describing this process is given by

$$\ddot{x}(t) + \omega_0^2 x(t) = -2\beta\dot{x}(t) + \xi(t). \quad (7)$$

The parameter $\beta \geq 0$ represents the contribution of frictional or viscous dissipation, the frequency ω_0 is the natural frequency of the noise free and dissipation free system ($\xi(t) = \beta = 0$), and the white noise forcing $\xi(t)$ is like that in the Brownian process example. Section A.2 in the Appendix discusses the stationary statistics for this process. The remainder of this section describes the problem of forecasting and characterizing the predictability of this system when it is underdamped; i.e., $\Omega^2 \equiv \omega_0^2 - \beta^2 > 0$.

3.2.1 The optimal forecast

As in the last subsection, since the process is linear and Gaussian, the optimal forecast (also the most probable future state) is the same as the mean of an infinite ensemble; i.e., it is the noise free solution of (7) whose initial conditions are the state and time tendency at the moment of the last measurement. The forecast satisfying these conditions is given by

$$x_{dhp}(\tau) = \frac{e^{-\beta\tau}}{\Omega} \{x(0)\Omega \cos(\Omega\tau) + [\dot{x}(0) + \beta x(0)] \sin(\Omega\tau)\}. \quad (8)$$

The optimal forecast (8) will be called *damped harmonic persistence* in analogy with the damped persistence forecast given by (2). Note that for certain initial conditions relevant for the growing phase of an oscillation, the damped harmonic persistence forecast results in an initially growing anomaly. This growth is in contrast to the damped persistence forecast (2) which always results in a damping of anomalies and hence can never capture a growing anomaly. Once the initial state $x(0)$ and time tendency $\dot{x}(0)$ are measured, the damped harmonic persistence forecast can be constructed after the damping coefficient β and natural frequency ω_0 are estimated from the *acf* of a climatology.

The mean squared error in the damped harmonic persistence forecast $\sigma_{dhp}^2 = \langle (x(\tau) - x_{dhp}(\tau))^2 \rangle$ [which is also the ensemble variance where each ensemble element starts with the same $x(0)$ and $\dot{x}(0)$] is given by

$$\sigma_{dhp}^2(\tau) = \langle x^2 \rangle \left\{ 1 - \frac{e^{-2\beta\tau}}{\Omega^2} [\omega_0^2 - \beta^2 \cos(2\Omega\tau) + \beta\Omega \sin(2\Omega\tau)] \right\}. \quad (9)$$

The error σ_{dhp}^2 exponentially saturates to the climatological variance $\langle x^2 \rangle = \sigma_\xi^2 / (4\beta\omega_0^2)$. The corresponding error for the persistence forecast $x_{persist} = x(0)$ is

$$\sigma_{persist}^2(\tau) = 2 \langle x^2 \rangle \left\{ 1 - e^{-\beta\tau} \left[\cos(\Omega\tau) + \frac{\beta}{\Omega} \sin(\Omega\tau) \right] \right\}, \quad (10)$$

which saturates to twice the climatological variance and is always larger than the damped harmonic persistence forecast error.

Both forecast errors oscillate due to the oscillatory nature of the process. For the cases considered in this paper, this oscillation is not so apparent because of the dominance of the exponential prefactor. The slope of the optimal forecast error is given by

$$\frac{d\sigma_{dhp}^2}{dt} = \frac{4\beta\omega_0^2 \langle x^2 \rangle}{\Omega^2} e^{-2\beta\tau} \sin^2(\Omega\tau), \quad (11)$$

which vanishes at zero lead time. Recall the slope (6) for the error made in the optimal forecast of the Brownian process (the damped persistence forecast) is $2\alpha \langle v^2 \rangle$ at zero lead time.

It is illustrative to compare the times at which the errors in the damped harmonic persistence and pure persistence forecasts reach some subjective fraction of the climatological variance. For example, consider a harmonic Brownian process of period 33 years and decay time 10 years, which correspond to values estimated from the coupled model *acf* in Figure 2. The error in the damped harmonic persistence forecast (9) of this process takes 7.2 years to reach 50% of the climatological variance and 9.7 years to reach 75%. The pure persistence forecast error (10) reaches 50% after 4.4 years and 75% after 5.6 years.

3.2.2 A numerical example

Figure 7A shows a 200 year realization of the harmonic Brownian process. The model parameters are indicated in the caption. The *acf* from a 400 year realization is shown in Figure 7B. Figure 8A shows a nine element ensemble. The ensemble mean is shown in Figure 8B along with a damped harmonic persistence fit given by equation (8). Figure 8C shows the ensemble variance. The smoother dashed line is the variance (9) from the damped harmonic persistence forecast.

4 Linear predictability in a THC box model

4.1 Introduction

In this section, the previous study of variability generated by Brownian and harmonic Brownian processes will be used to help guide our characterization of the variability seen in a white noise driven THC box model. Such a study provides the next level in a hierarchy of models for studying the variability of the coupled model's THC. Box models are low order systems which have proven to be of use for understanding the stability and variability of the North Atlantic THC. The model of interest here is an extension of the familiar advective two-box model of Stommel (1961) to that of four boxes. The focus in this section, as in the preceding discussion, is on the variability of the box model around some stable stationary state. The evolution of Stommel-type (Stommel 1961, Welander 1986) box models are determined by conservation laws of salinity and heat applied to various well mixed regions or boxes. In their canonical form, the only nonlinearity occurs in advection terms if the equation of state for sea water is taken as a linear function of temperature and salinity: $\rho_i = \rho_0[1 - \alpha_T(T_i - T_0) + \beta_S(S_i - S_0)]$ with ρ_0 , T_0 , and S_0 being reference density, temperature, and salinity, respectively. The thermal and saline expansion coefficients α_T and β_S , whose dimensions are $^{\circ}\text{K}^{-1}$ and psu^{-1} , respectively, are taken as constants throughout the model which guarantees that the advective circulation vanishes when the north/south temperature and salinity gradients vanish. Hence, the circulation is driven solely by horizontal pressure gradients between the north and south which, using the hydrostatic approximation, correspond to horizontal density gradients. More realistic nonlinear equations of state are thought to give no qualitative change in the model's behaviour under the moderate variability considered here.

GT95 argued for the ability of a particular two dimensional, mixed boundary condition four-box model to emulate the coupled model's THC variability and the zonally averaged circulation variability. The same box model, without stochastic forcing, was previously considered by Huang et al. (1992) and Tziperman et al. (1994). As shown in GT95, it is the excitation of a damped oscillatory eigenmode by random atmospheric forcing, modeled as white noise, which is important for characterizing the low frequency box model variability. Coupled to this damped oscillatory mode are purely damped modes which are also of relevance to establishing the model's predictability.

The experiments shown here are the result of numerically integrating the nonlinear conservation equations given in GT95. The numerical scheme described in Penland (1989) is employed using 365 time steps per model year.

4.2 The four box model

Figure 9 shows the configuration of the four-box model. The model parameters, described further in GT95, are given in the caption. The temperature and salinity of each box are time dependent hence providing eight degrees of freedom.

Linearization of the mixed boundary condition box model governing equations about a stable thermally dominant steady state, realized using the parameters given in Figure 9 with restoring boundary conditions on both temperature and salinity, yields a damped oscillatory eigenmode of period 62 years and decay time 10 years, respectively, as well as purely damped modes. Since the linear system is not self-adjoint, the eigenmodes are coupled to one another. The box model steady state, and its variability, were tuned to emulate that seen in the coupled model.

Figure 10 shows 400 years of yearly averaged four box model circulation driven by a white noise surface heating. It is this time series which is used as a climatology necessary to quantify predictability of the subsequent box model ensemble experiments. Also shown is the signal after applying a 10 year low pass filter. Low passing highlights the response due to the low frequency damped harmonic eigenmode as discussed in GT95.

Figure 11 shows the *acf* for the box model's THC as well as fits by the *acf* for the Brownian and harmonic Brownian processes. Note the broad trough in the box model's *acf* which is similar to that in *acf* of the coupled model THC index (Figure 2). As in the coupled model, the statistical significance of the trough is marginal at the 95% confidence level. However, for the box model, a direct analysis of the model's linearized dynamics supports our interpreting the trough as a contribution to the model's variability from a damped oscillatory THC eigenmode. The *acf* from substantially longer time series also supports this view. It is straightforward to verify, through box model experiments in which the oscillatory eigenmode is either more or less damped, that the breadth and depth of the trough is related to the rather large damping of the oscillatory eigenmode, the presence of the purely damped eigenmodes to which the oscillatory mode is coupled, and sampling errors. The correspondence of the box model's circulation statistics to that of the coupled model's THC index, as well as the general correspondence between the zonally averaged mechanisms acting in the two models as studied by GT95, motivate a stochastic interpretation for the coupled model's THC variability similar to that acting in the box model.

4.3 Four-box model THC predictability

We now characterize the predictability of the THC variability simulated by the stochastically forced box model. In this analysis, it will be of interest to quantify the predictability of the lower frequency variability which is largely associated with the damped oscillatory mode in addition to the predictability of the yearly averaged variability. For obtaining predictability of the low frequency variability, it will be necessary to low pass filter the ensemble elements in order to remove some of the effects of the faster de-correlating purely damped eigenmodes which are coupled to the damped oscillatory mode. Note that due to the coupling of the modes, filtering cannot completely isolate the behaviour of the oscillatory mode. Therefore, predictability even of the filtered process will be affected by the purely

damped modes as well as the damped oscillatory mode. The same 10 year low pass filtering that has been applied to the climatologies shown in Figures 1 and 10 will be applied to the ensemble elements. For the ensemble experiments considered here and in the coupled model, a 10 year low pass filter is quite drastic due to the relatively short length of the experiments (30 years). Also, as mentioned in Section 2.2, filtering increases the e-folding time of the auto-correlation for a damped stochastic process. It follows that the predictability of the filtered process will be increased. In the interests of providing some sense of the added predictability associated with such a filtering, and since this particular low pass filter was seen in DMS93 and GT95 to provide a useful means of highlighting the low frequency THC variability in the coupled and box models, we present an analysis of both the yearly averaged and filtered yearly averaged THC ensemble experiments.

Figure 12A shows the yearly averaged circulation for a nine element ensemble experiment from the four box model. The results are compared in Figure 12B to that from particular Brownian and harmonic Brownian processes, which are specified from measurements of the initial position and slope of the ensemble and parameters estimated from the *acf* in Figure 11. The ensemble mean relaxes to zero in rough accordance with both the mean of an infinite ensemble of Brownian and harmonic Brownian processes, i.e., the damped persistence and damped harmonic persistence forecasts. Note, however, that the small oscillation expected from the damped harmonic persistence forecast is not manifested in the box model ensemble. Apparently, the damping of the damped oscillatory eigenmode, and its coupling to the purely damped processes (recall the system is not self-adjoint), act to suppress the oscillation expected if the damped oscillatory mode acted in isolation.

The initial rapid growth in the ensemble variance shown in Figure 12C agrees with the growth expected from the ensemble variance in a Brownian process. This result is interpreted as due to the presence of the rapidly de-correlating non-oscillatory modes. Also shown is the ensemble after artificially extending the initial point 10 years to its past and then applying a 10 year low pass filter. The closer agreement of the finite sized filtered ensemble statistics with the damped harmonic persistence solution, especially the initial growth in ensemble variance, is apparent and can be expected based on our characterization of the growth in ensemble variance for the harmonic Brownian process in Section 3.2.1 [in particular equation (11)].

4.4 Four-box summary

Although the four-box model contains advective nonlinearities, its variability as driven by a moderate amplitude white noise forcing can be understood effectively as that of a system of Brownian processes coupled to a single harmonic Brownian process. The coupling arises from the non-self-adjointness of the linearized system. The damped oscillatory eigenmode is responsible for the negative trough in the *acf* shown in Figure 11. The purely damped modes and sampling errors in turn act to broaden

this trough and the damping of the oscillation determines the depth of the trough. The natural extension of the linear stochastic theory to the present system of coupled modes also forms a useful theoretical framework for understanding the predictability of the box model's THC variability. Of particular note is the rather damped behaviour of the ensemble mean in which there is no significant oscillatory behaviour. This result is consistent with larger ensemble sizes and is the result of the relatively large damping of the damped oscillatory eigenmode along with its being coupled to purely damped modes. Filtering, as expected, reduces the initial growth of the ensemble variance which brings it somewhat more in line with the variance from an ensemble of harmonic Brownian processes. Box model experiments (not shown) in which the damped oscillatory eigenmode is less damped, and hence more dominant in the model's variability, bring out the oscillatory mode in the ensemble mean and correspondingly increase the predictability of the circulation.

Some numbers are useful to establish the time scales for predictability in this model. The ensemble variance from the yearly averaged THC, which acts over short time scales much as an ensemble of red noise processes, reaches a variance 50% that of the climatology after roughly 1.5 years. This time can be used to define a predictability time scale for the yearly averaged signal from this model. The variance of the filtered ensemble reaches 50% that of the filtered climatology after roughly 5-7 years.

5 The coupled model ensemble statistics

Following the previous analysis of the four-box model's THC predictability, the linear stochastic framework is used to help interpret the statistics from the coupled model ensemble experiments of Section 2. Figure 13 shows the first ensemble experiment from Figure 3 along with the ensemble mean and ensemble variance. Both the yearly averaged and 10 year low pass signals are shown.

The mean of the infinite sized ensemble of Brownian and harmonic Brownian processes, which initial conditions estimated from the coupled model ensembles, are superposed with the ensemble mean. The decay times and periods for these forecasts were approximated from the *acfs* of the climatology in Figure 2A,B. Based on our previous experience with the Brownian and harmonic Brownian processes and their applications to the box model, Figure 13 indicates that the behaviour of the THC simulated in the coupled model is consistent with the linear theory much in the same fashion as seen in the box model results. The second ensemble, shown in Figure 14, indicates the same consistency.

The ensemble variance of the yearly averaged signal, which increases in time similar to the variance from a red noise ensemble, reaches 50% of the climatological variance after approximately 1.5 years. This time defines a time scale for the predictability of the yearly averaged THC index from the coupled model. The ensemble variance of the low pass signals reaches 50% of the climatological variance

after approximately 5-7 years. This time defines a time scale for the predictability of the interdecadal THC variability from the coupled model.

6 Discussion and conclusions

A system for monitoring the Atlantic Ocean does not yet exist, but is under active study by a number of large-scale research programs. This coupled model study represents a preliminary attempt to assess the potential of using such an observational system to predict North Atlantic climate variability on decadal to multi-decadal time scales. In particular, this investigation reported results of two sets of 30 year ensemble predictability experiments carried out with the GFDL coupled ocean-atmosphere GCM. A multi-century integration of the model was used as a climatology to which to compare the ensemble statistics. The ensemble members possess identical oceanic initial conditions with randomly chosen atmospheric initial conditions taken from the model climatology. The motivation for choosing this ensemble design stems from the hypothesis that it will provide an upper limit to the model's predictability and hence is useful as a benchmark for comparing more realistic predictability experiments. Due to the connection between the model's North Atlantic climate variability and its THC, the predictability of the model's THC index variability was characterized. This index represents the magnitude of the THC in the model's North Atlantic.

A case study using a mixed boundary condition four-box model of the meridional THC motivated a particular linear stochastic interpretation of the coupled model's THC variability. This box model, unlike the prototype model of Stommel (1961), contains a linear damped oscillatory mode for a stable state corresponding to the present North Atlantic in which temperature dominates the north-south density gradient (GT95). In addition, it contains purely damped modes. The damping of the oscillatory mode is related to the strength of the steady state salinity forcing with a larger forcing bringing the model into a more oscillatory regime. The regime corresponding to the variability of the coupled model is relatively damped. The box model's variability can be interpreted with the help of two single variable linear stochastic processes; namely, the Brownian process (red noise) and the harmonic Brownian process (noise driven damped harmonic oscillator). The model's red noise response corresponds to the behaviour of the rapidly de-correlating portion of the THC climatology as indicated its *acf* shown in Figure 11. The damped harmonic oscillator response corresponds to the longer time or low frequency behaviour of the THC indicated by the *acf*'s tendency to exhibit a damped oscillatory response as seen by the presence of a negative trough. The damping of the oscillatory behaviour is quite large, however, and the statistical significance is therefore marginal and must be supported by direct analysis of the model's linearized dynamics. Longer time series support this interpretation. Since the linearized box model is not self-adjoint, the model can be thought of as a system of Brownian processes coupled to a single harmonic Brownian process.

The box model provides a useful case study for applying the basic ideas of linear stochastic variability and predictability discussed in Section 3. As the statistics from both the box model and coupled model are quite similar, and based on our belief that the physical mechanisms responsible for the box model's variability are related to those seen in a zonally averaged sense from the coupled model (as argued in GT95), the interpretation of the coupled model's THC variability and its statistics follows directly from that of the box model. This interpretation leads us to believe that longer ensemble experiments with this model will not alter the predictability time scales determined in Section 5 for the coupled model's THC variability.

The linear stochastic perspective as applied the coupled model's THC variability suggests that the oceanic variability in the coupled model is largely driven by atmospheric variability. Therefore, the model's THC predictability relies on the ocean's ability to maintain memory under the effects of this nearly random forcing. The stochastic interpretation of this variability is broadly consistent with that embodied in the stochastic models of Hasselmann (1976,1982), Mikolajewicz and Meier-Reimer(1990), Weisse et al. (1994), Bryan and Hansen (1994) and GT95. The work of Penland and Sardeshmukh (1994) points to the relevance of such a perspective for ENSO forecasting.

Even with the very long time scales of the coupled model's North Atlantic climate variability (40–60 years), the rather small predictability time scale (1.5–7 years) is not unexpected given the noise driven stochastic interpretation and the rather damped behaviour of the model's variability. This situation can be compared to the roughly one year predictability limit for the 4–7 year time scale ENSO variability (Neelin et al. 1994). The large differences in relative time scales arise from the very different physical mechanisms acting in the two forms of ocean-atmosphere variability. However, in absolute terms the model's THC predictability time scales are somewhat encouraging from a forecasting perspective, assuming they are not drastically reduced with more realistic ensemble experiments in which the oceanic state is perturbed. Furthermore, although a surface to deep water monitoring system is probably justified as a means to monitor global climate change, the present results might provide an additional justification for such a mid-latitude observing system, particularly in the North Atlantic.

Although the low order stochastic models discussed in this work are concise and therefore of value from a conceptual standpoint, extensions to this work are necessary before it is of practical use for a forecasting system using a coupled GCM. Namely, the THC index is not a readily measurable quantity in the real ocean and as such should be correlated with an observable field. As shown by DMS93, such an observable in the model is the dynamic topography since it is related through geostrophy to the meridional overturning. An analysis similar to that presented here, replacing the THC index time series with that of the first few dynamic topography EOFs, can be carried out. It is expected that the conclusions reached here concerning the linear noise driven nature of the system would remain unchanged. However, the utility of understanding the predictability of EOF patterns would

aid in addressing practical issues such as designing an observational network for the initialization and monitoring necessary for a forecasting system. Such a study would be a natural extension of the current research. Furthermore, it should be noted that the model's THC variability exhibits only a moderate amount of variability ($\approx 5\% - 10\%$ of the roughly 20 Sv mean meridional circulation) as it appears to be quite damped. Real world measurements would be hard pressed to capture variability of this scale. These limitations hence motivate studies of the variability in other realistic coupled models in order to understand if this is a limit to the real coupled ocean-atmosphere system or is somewhat model dependent. It should be noted that a severe limitation of the current coupled GCMs is their coarse resolution which is far from resolving oceanic mesoscale eddies. It remains a topic of future research to assess the effects these eddies have on long term oceanic predictability.

From an observational perspective, the need to estimate such climatological statistics as the auto-correlation function of the long time scale processes simulated here places a heavy burden on the limited climate data. The paucity of available data should further motivate the continuing accumulation of paleoclimate proxy data for the North Atlantic as well as to motivate the establishment of long term climate monitoring networks. With the accumulation of long time records, validation of models is more available which improves our confidence in their climatology and ultimately their forecasts.

A Appendix

In this appendix, we present the stationary statistics of the Brownian and harmonic Brownian processes. More elaboration of these processes useful for the derivations in this appendix can be found in the books by Gardiner (1985) and Kubo et al., (1985).

A.1 The Brownian process

The Brownian process is defined by equation (1), which is reproduced here for completeness:

$$\dot{v}(t) = -\alpha v(t) + \xi(t). \quad (12)$$

A particular solution can be formally written

$$v_p(t) = \int_{-\infty}^t e^{-\alpha(t-u)} \xi(u) du. \quad (13)$$

For the subtleties of interpreting the integral of white noise, refer to Gardiner (1985). Choosing the lower limit at $-\infty$ for the particular solution allows the stationary statistics of the process to be found straightforwardly from this expression. The stationary mean $\langle v \rangle$ of the process vanishes. The

stationary auto-covariance function (*acf*) can be found by multiplying $v_p(t)$ by $v_p(s)$ and taking an ensemble mean. The result for $s < t$ is

$$\langle v(t)v(s) \rangle = (\sigma_\xi^2/2\alpha) \exp[-\alpha(t-s)]. \quad (14)$$

The covariance between adjacent points in time falls off exponentially with e-folding time $1/\alpha$. Note the dependence on the time difference $(t-s)$; a property characteristic of statistically stationary processes. Setting $t=s$ gives the time independent zero lag variance

$$\langle v^2 \rangle = (\sigma_\xi^2/2\alpha). \quad (15)$$

As expected, the larger the damping coefficient α , the smaller the variance; conversely, the larger σ_ξ^2 , representing the power of the noise forcing, the larger the variance. The normalized auto-covariance

$$\langle v(t)v(s) \rangle \langle v^2 \rangle^{-1} = \exp[-\alpha(t-s)] \quad (16)$$

is called the auto-correlation function (*acf*). This damped exponential has been fit to the *acf* for the processes throughout this paper.

The Fourier transform of (1) yields the frequency space solution $v(\omega) = \xi(\omega)/(\alpha + i\omega)$. Since the noise is white, $\xi(\omega) = \sigma_\xi$. The absolute square $|v(\omega)|^2$ gives the spectrum $S(\omega) = 2\alpha\langle v^2 \rangle/(\alpha^2 + \omega^2)$. The form of the spectrum motivates the name *red noise* since the power is concentrated in the low or red frequency end of the spectrum. Note that the e-folding time α^{-1} of the *acf*, above which there is basically no correlation or memory remaining in the process, corresponds to the angular frequency $\omega = \alpha$, below which the spectrum flattens out to approximate that of a white noise process with power $2\langle v^2 \rangle \alpha^{-1} = \sigma_\xi^2/\alpha^2$.

A.2 The harmonic Brownian process

The harmonic Brownian process is described by

$$\ddot{x}(t) + \omega_0^2 x(t) = -2\beta \dot{x}(t) + \xi(t). \quad (17)$$

Setting $\beta^2 < \omega_0^2$ allows the noise free system to exhibit a damped harmonic response. For the opposite inequality, the motion is overdamped. Solutions for the overdamped case can be found from the following underdamped solutions through analytic continuation. The noise free solution in equation (8). This solution is also the ensemble mean of the process and it vanishes in the stationary limit. A particular solution to (17) is

$$x_p(t) = \int_{-\infty}^t \frac{e^{-\beta(t-u)}}{\Omega} \sin[(\Omega(t-u))] \xi(u) du. \quad (18)$$

The *acvf* is given by

$$\langle x(t)x(s) \rangle = \langle x^2 \rangle e^{-\beta(t-s)} \left\{ \cos[\Omega(t-s)] + \frac{\beta}{\Omega} \sin[\Omega(t-s)] \right\}, \quad (19)$$

where the lag $(t-s) > 0$. For $(t-s) < 0$, the solution takes the same form with an absolute value on the lag. Setting $t = s$ yields the zero lag variance of the process $\langle x^2 \rangle = \sigma_\xi^2 / (4\beta\omega_0^2)$. The *acf* $\langle x(t)x(s) \rangle \langle x^2 \rangle^{-1}$ is that function which is fit to the sample *acfs* throughout this paper.

The Fourier transform of the *acvf* gives the spectrum

$$S_{ho}(\omega) = \langle x^2 \rangle \frac{4\beta\omega_0^2}{4\beta^2\omega^2 + (\omega_0^2 - \omega^2)^2}. \quad (20)$$

The spectrum has a peak value of $\langle x^2 \rangle \beta^{-1}$ at the angular frequency $\omega = \omega_0$, becomes the constant $4\beta \langle x^2 \rangle \omega_0^{-2}$ at zero frequency, and falls off as ω^{-4} for frequencies $\omega \gg \beta$. Note that the spectrum peaks at the oscillator's natural angular frequency ω_0 whereas the *acvf* (19) oscillates with the reduced frequency $\Omega = (\omega_0^2 - \beta^2)^{1/2}$.

A.3 Comparison of the stationary statistics

For the harmonic Brownian process, the high frequency behaviour of the spectrum and the small time lag behaviour of the *acf* are distinct from the corresponding behaviour of the Brownian process. Namely, the Brownian process correlation falls off immediately at non-zero lag time whereas the harmonic Brownian process decays less rapidly at such lags. This result has its complementary behaviour in frequency space with a faster decay at high frequency for the harmonic process. The low frequency and long lag time behaviour of the processes are equivalent as they both approximate the behaviour of white noise processes in this limit.

The above behaviours manifest in the form of the growth in error curves for the optimal forecasts of the two processes. Namely, the error in the damped persistence forecast of the Brownian process has a nonzero initial slope (equation (6)) corresponding to the sharper drop in small lagged correlation for the process. The damped harmonic persistence forecast of the harmonic Brownian process has a zero initial error slope (equation (11)) corresponding to the slower initial de-correlation of the harmonic process.

Acknowledgments.

This work would not have been possible without the generous support and guidance of Tom Delworth, Ron Stouffer, and Eli Tziperman. We thank them wholeheartedly. Further beneficial discussions and advice were provided by Jeff Anderson, Bhupendra Goswami, Alex Hall, Isaac Held,

Syukuro Manabe, and Cecile Penland. Thanks also go to GFDL, and especially its Ocean Group, who kindly provided us with the Cray-YMP time necessary to conduct this research. Funding for SMG is provided by a fellowship from the NOAA Postdoctoral Program in Climate and Global Change and NOAA's Geophysical Fluid Dynamics Laboratory. Support was also provided by Atlantic Climate Change Program funding from NOAA's Office of Global Change.

B References

- J.L. Anderson and W.F. Stern, 1995: Evaluating the predictive utility of ensemble forecasts in a perfect model setting. Preprint.
- Bjerknes, J. 1964: Atlantic air-sea interaction. *Advances in Geophysics*, **10**, 1-82.
- Broecker, W.S., D.M. Peteet and D. Rind, 1985: Does the ocean-atmosphere system have more than one stable mode of operation? *Nature*, **315**, 21–26.
- Bryan, F., 1986: High-latitude salinity effects and interhemispheric thermohaline circulations. *Nature*, **323**, 301–304.
- Bryan, K. and F.C. Hansen, 1994: A stochastic model of North Atlantic climate variability on a decade to century time-scale. *Proceedings of the Workshop on Decade-to-Century Time Scales of Climate Variability*, National Research Council, Board on Atmospheric Sciences and Climate, National Academy of Sciences, Irvine, CA.
- Bryan, K. and R. Stouffer, 1991: A note on Bjerknes' hypothesis for North Atlantic variability. *Journal of Marine Systems*, **1**, 229-241.
- Deser, C. and M.L. Blackmon, 1993: Surface climate variations over the North Atlantic Ocean during Winter: 1900–1989. *Journal of Climate*, **6**, 1743–1753.
- Gardiner, C.W., 1985: *Handbook of Stochastic Methods for Physics, Chemistry, and the Natural Sciences*. Springer-Verlag.
- Goswami, B. N. and J. Shukla, 1991: Predictability of a coupled ocean-atmosphere model, *Journal of Climate*, **4**, 3–22.
- Griffies, S.M. and E. Tziperman, 1995: A linear thermohaline oscillator driven by stochastic atmospheric forcing. *Journal of Climate* submitted.
- Hasselmann, K., 1976: Stochastic climate models, part 1—theory. *Tellus*, **18**, 473-484.
- Hasselmann, K., 1982: An ocean model for climate variability studies. *Progress in Oceanography*, **11**, 69–92.
- Huang, R.X., J.R. Luyten, and H.M. Stommel, 1992: Multiple equilibria states in combined thermal and saline circulation. *J. Phys. Oceanogr.*, **22**, 231–246.
- Kleeman, R. and S.B. Power, 1994: Limits to predictability in a coupled ocean-atmosphere model due to atmospheric noise. *Tellus*, **46A**, 529–540.

- Kloeden, and Platen, 1992: *Numerical Solution of Stochastic Differential Equations*, Springer-Verlag.
- Kubo, R., M. Toda, and N. Hashitsume, 1985: *Statistical Physics II*, Springer-Verlag.
- Kushnir, Y., 1994: Interdecadal variations in North Atlantic sea surface temperature and associated atmospheric conditions. *Journal of Climate*, **7**, 141–157.
- Levitus, S., 1989a: Interpentadal variability of temperature and salinity at intermediate depths of the North Atlantic Ocean, 1970-1974 versus 1955–1959. *Journal of Geophysical Research*, **94**, 6091–6131.
- Levitus, S., 1989b: Interpentadal variability of salinity in the upper 150m of the North Atlantic Ocean, 1970-1974 versus 1955–1959. *Journal of Geophysical Research*, **94**, 9679–9685.
- Levitus, S., 1990: Interpentadal variability of steric sea level and geopotential thickness of the North Atlantic Ocean, 1970-1974 versus 1955–1959. *Journal of Geophysical Research*, **95**, 5233–5238.
- Lorenz, E., 1969: Three approaches to atmospheric predictability. *Bulletin of the American Meteorological Society*, **50**, 345-349.
- Lorenz, E., 1973: On the existence of extended range predictability. *Journal of Applied Meteorology*, **12**, 543–546.
- Manabe, S., and R.J. Stouffer, 1988: Two stable equilibria of a coupled ocean-atmosphere model. *Journal of Climate*, **1**, 841–866.
- Manabe, S., and R.J. Stouffer, 1995: Low frequency variation of surface air temperature in a 1000 year integration of a coupled ocean-atmosphere model. Submitted to *Journal of Climate*.
- Manabe, S., R.J. Stouffer, M.J. Spelman, and K. Bryan, 1991: Transient response of a coupled ocean-atmosphere model to gradual changes of atmospheric CO_2 : Part I: Annual mean response. *Journal of Climate*, **4**, 785–818.
- Manabe, S., M.J. Spelman, and R.J. Stouffer, 1992: Transient response of a coupled ocean-atmosphere model to gradual changes of atmospheric CO_2 : Part II: Seasonal response. *Journal of Climate*, **5**, 105–126.
- Mysak, L.A., T.F. Stocker, and F. Huang, 1993: Century-scale variability in a randomly forced, two-dimensional thermohaline ocean circulation model. *Climate Dynamics*, **8**, 103–116.

- Mikolajewicz, U., and E. Maier-Reimer, 1990: Internal secular variability in an ocean general circulation model. *Climate Dynamics*, **4**, 145–156.
- Mikolajewicz, U. and E. Maier-Reimer, 1994: Mixed boundary conditions in ocean general circulation models and their influence on the stability of the model's conveyor belt. *Journal of Geophysical Research*, **99**, 22633–22644.
- W.H. Munk, 1960: Smoothing and persistence. *Journal of Meteorology*, **17**, 92–93.
- Neelin, D.J., M. Latif, and F-F. Jin, 1994: Dynamics of coupled ocean-atmosphere models: the tropical problem. *Annual Review of Fluid Mechanics*, **26**, 617–659.
- Penland, C., 1989: Random forcing and forecasting using principal oscillation pattern analysis. *Monthly Weather Review*, **117**, 2165–2185.
- Penland, C. and P.D. Sardeshmukh, 1994: The optimal growth of tropical sea surface temperature anomalies. *Journal of Climate* submitted.
- Power, S., F. Tseitkin, M. Dix, R. Kleeman, R. Colman, and D. Holland, 1995: Stochastic variability at the air-sea interface on decadal time-scales. Preprint.
- Rahmstorf, S., 1994: Rapid climate transitions in a coupled ocean-atmosphere model. *Nature*, **372** 82–85.
- Reif, F., 1965: *Fundamentals of statistical and thermal physics*, McGraw-Hill.
- Sausen, R., K. Barthel, and K. Hasselmann, 1988: Coupled ocean-atmosphere models with flux correction. *Climate Dynamics*, **2** 144–163.
- Schlesinger, M.E. and N. Ramankutty, 1994: An oscillation in the global climate system of period 65–70 years. *Nature*, **367**, 723–726.
- Stommel, H., 1961: Thermohaline convection with two stable regimes of flow. *Tellus*, **13**, 224–230.
- Stouffer, R. J., S. Manabe, and K. Bryan, 1989: Interhemispheric asymmetry in climate response to a gradual increase of atmospheric CO_2 . *Nature*, **342**, 660-662.
- Stouffer, R. J., S. Manabe, and K. Ya. Vinnikov, 1994: Model assessment of the role of natural variability in recent global warming. *Nature*, **367**, 634–636.
- Tziperman, E. and K. Bryan, 1993: Estimating global air-sea fluxes from surface properties and from climatological flux data using an oceanic general circulation model. *Journal of Geophysical Research*, **98**, 22629–22644.

- Tziperman, E., R. Toggweiler, Y. Feliks, and K. Bryan, 1994: Instability of the thermohaline circulation with respect to mixed boundary conditions: Is it really a problem for realistic models? *Journal of Physical Oceanography*, **24**, 217–232.
- Weaver, A.J. and T.M.C. Hughes, 1992: Stability and variability of the thermohaline circulation and its link to climate. *Trends in Physical Oceanography*, **1**, 15–70.
- Weisse, R., U. Mikolajewicz, and E. Maier-Reimer, 1994: Decadal variability of the North Atlantic in an ocean general circulation model. *Journal of Geophysical Research*, **89**, 12411–12421.
- Welander, P., 1986: Thermohaline effects in the ocean circulation and related simple models. *Large-Scale Transport Processes in the Oceans and Atmosphere*, D.L.T. Anderson and J. Willebrand, Eds., NATO ASI series, Reidel.
- Zhang, S., R.J. Greatbatch, and C.A. Lin, 1993: A re-examination of the polar halocline catastrophe and implications for coupled ocean-atmosphere models. *Journal of Physical Oceanography*, **23**, 287–299.

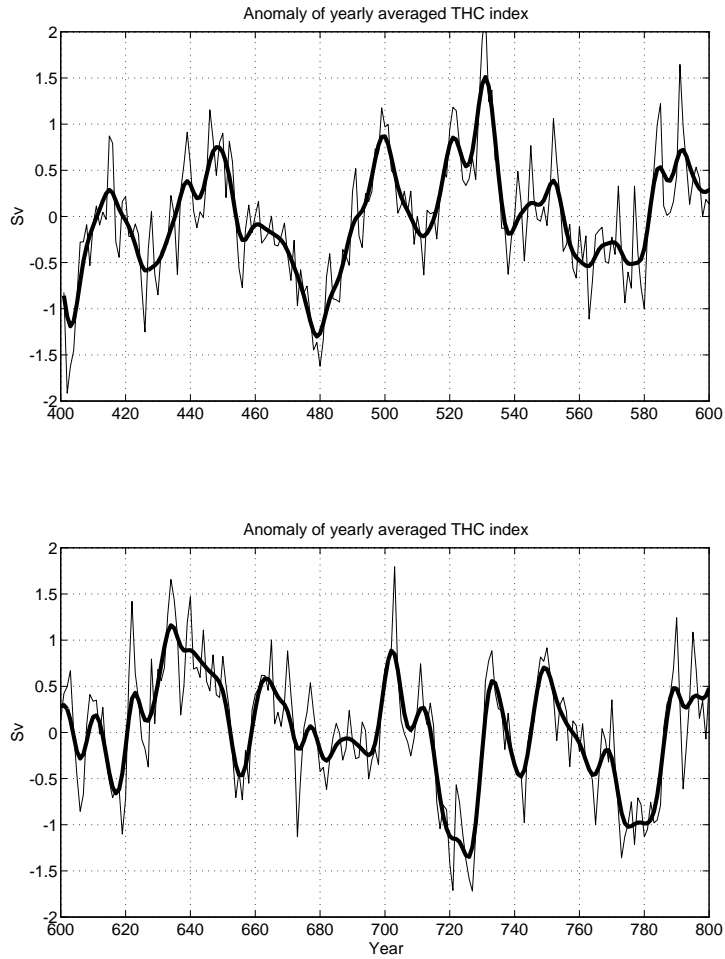


Figure 1: 400 years of linearly detrended anomalous yearly averaged THC index from the central portion of the coupled model experiment of DMS93 (thin solid line). This time series defines the climatology for use in quantifying the predictability exhibited by the ensemble experiments. The mean (subtracted out) and standard deviation are 18.1 Sv and .66 Sv ($1 \text{ Sv} = 10^6 \text{m}^3/\text{sec}$), respectively. Also shown is the time series after a 10 year low pass filtering has been applied (thick solid line). The standard deviation of the filtered time series is .54 Sv.

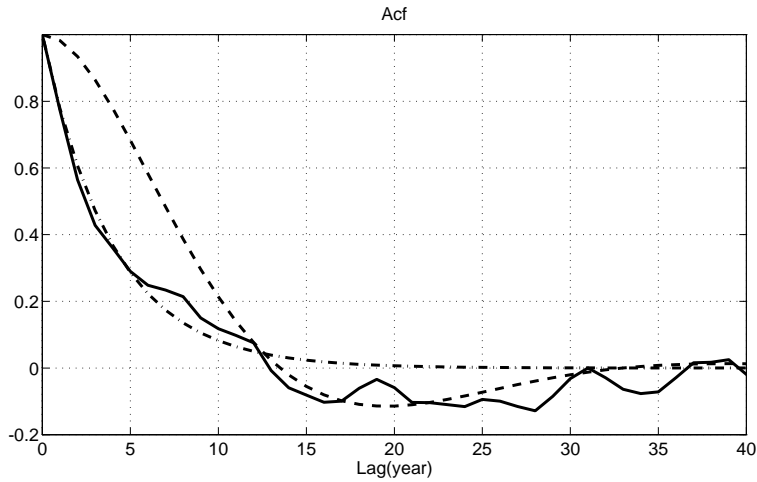


Figure 2: Auto-correlation function (*acf*) for the THC index shown in Figure 1. The smooth curves are fits of the *acf* from the Brownian or red noise process (dot-dashed line) with e-folding time of 4 years to the lags ≤ 10 years, and the *acf* from the harmonic Brownian process (dashed line) with period and e-folding time 31 and 9 years, to lags ≥ 10 years. A similar fit (not shown) to the *acf* of the low pass THC index time series gives a 7 year e-folding for the Brownian process and period and e-folding of 35 and 11 years, respectively, for the harmonic Brownian process.

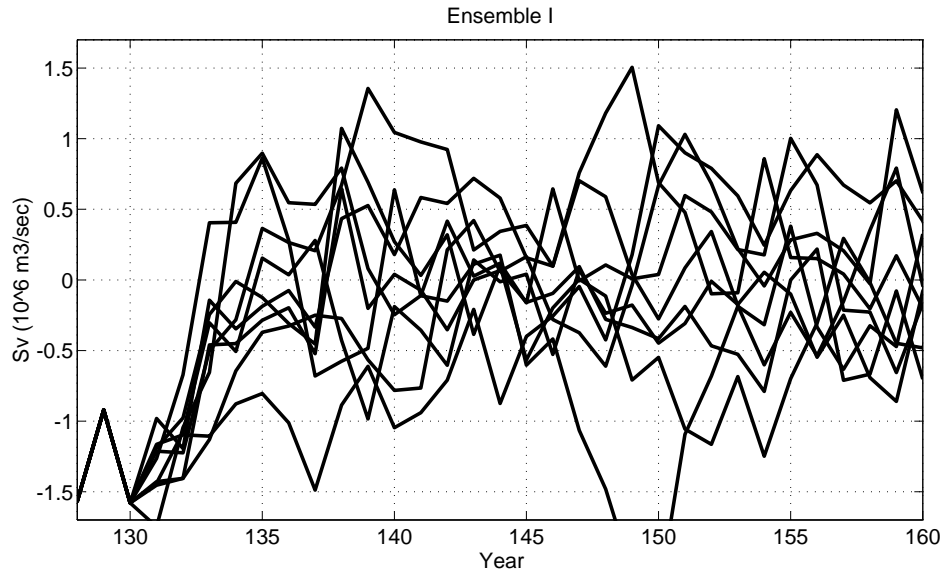


Figure 3: Nine element ensemble of yearly averaged anomalous THC index from the coupled model. Anomalies are defined relative to the mean of the linearly detrended 400 year climatology of Figure 1A. The ensemble starts at year 130 and extends for 30 years.

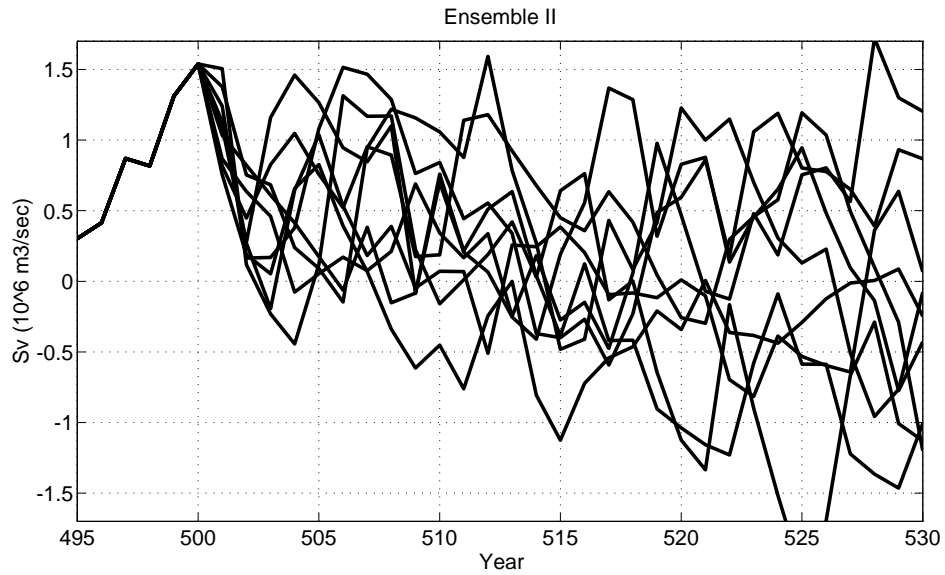


Figure 4: Same as Figure 3 for the ensemble starting from year 500 of the climatology.

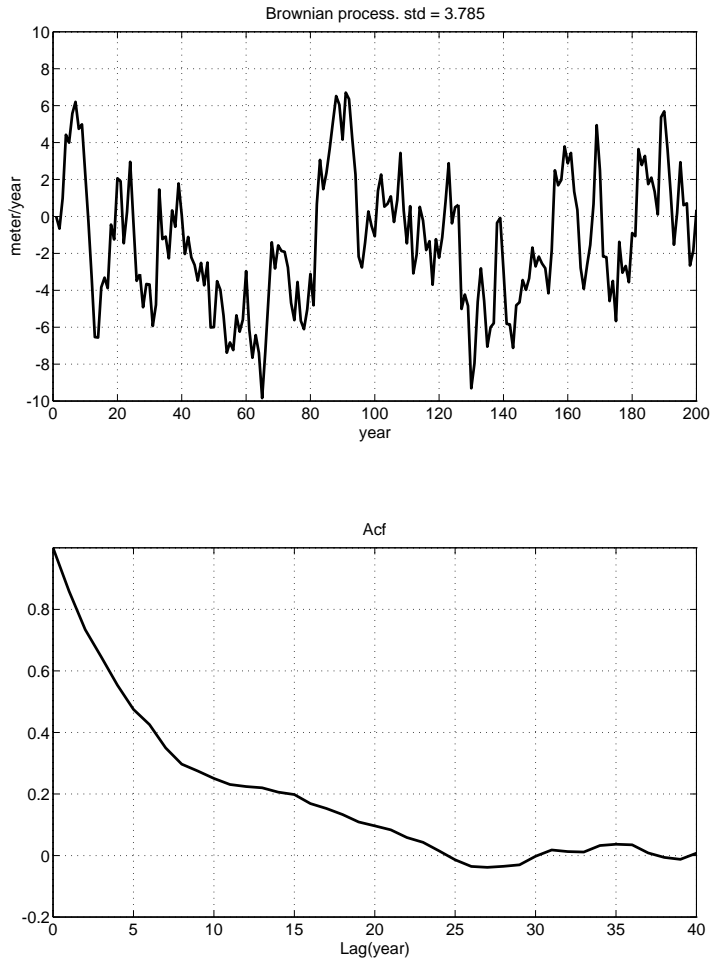


Figure 5: **(A)** A 200 year realization of the Brownian process [the continuous process is described by equation (1)] using an inverse damping time $\alpha^{-1} = 7$ years and noise variance $4 \text{ meter}^2/\text{years}^3$. The standard deviation of the process in the continuous case is 3.7 meter/year, and that realized in the numerical case is indicated on the figure title. **(B)** The *acf* of 400 years of the Brownian process, including the 200 years in **(A)**. This function approximates that from the infinite sized ensemble, which is a pure exponential decay, given by equation (14) in the Appendix. An ≈ 7 year e-folding time is apparent. Note that for illustrative purposes, we chose to set the dimensions of the process $v(t)$ to be those of a velocity, as is relevant for Brownian motion.

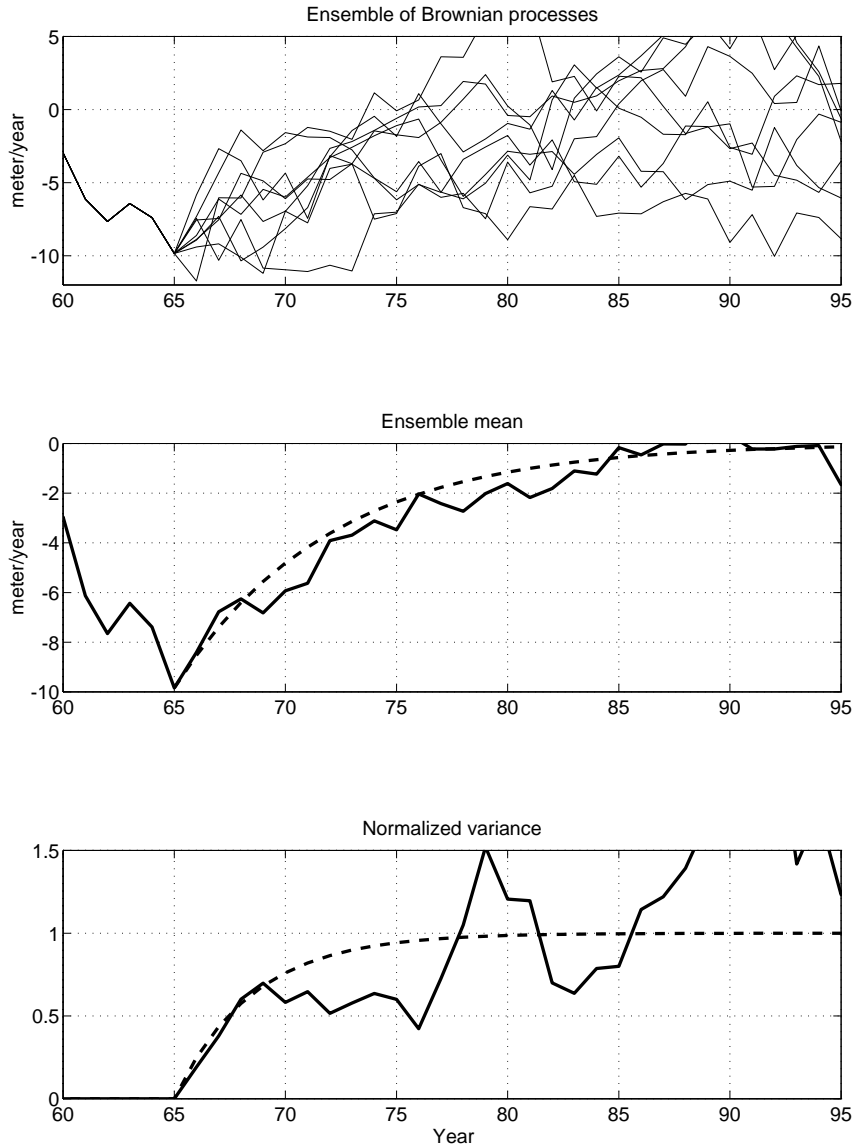


Figure 6: (A) A nine element ensemble of the Brownian process, each element of which has a different realization of the white noise process after starting from the same initial state near year 65. (B) The ensemble mean (solid line) and fit of the damped persistence [equation (2)]. Note the different vertical axis relative to (A). (C) The ensemble variance (solid line) and the error function [equation (4)] of the damped persistence forecast. Note the non-zero slope of the variance at zero lag consistent with equation (6).

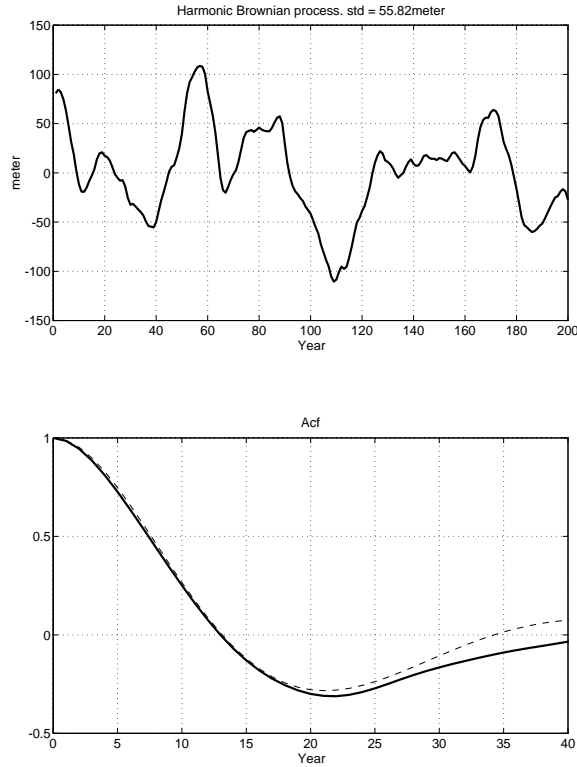


Figure 7: **(A)** A 200 year realization of the harmonic Brownian process [the continuous process is described by equation (7)] using an inverse damping time $\beta^{-1} = 10$ years, period $2\pi/\omega_0 = 33$ years. The standard deviation of the harmonic Brownian process in the continuous case is 52.5 meter. The realized standard deviation is indicated on the figure title. **(B)** The *acf* for 400 years of the harmonic Brownian process (solid line), including the 200 years of **(A)**. A least squares fit of the theoretical *acf* (equation (19) discussed in the Appendix) to the sample *acf* is the dashed line. The period and decay time from this fit are 39 and 17 years, respectively. Note the broadening of the trough relative to the theoretical *acf* can be attributed to sampling errors. The depth of the trough is related to the damping of the oscillation (more damping yields a shallower trough).

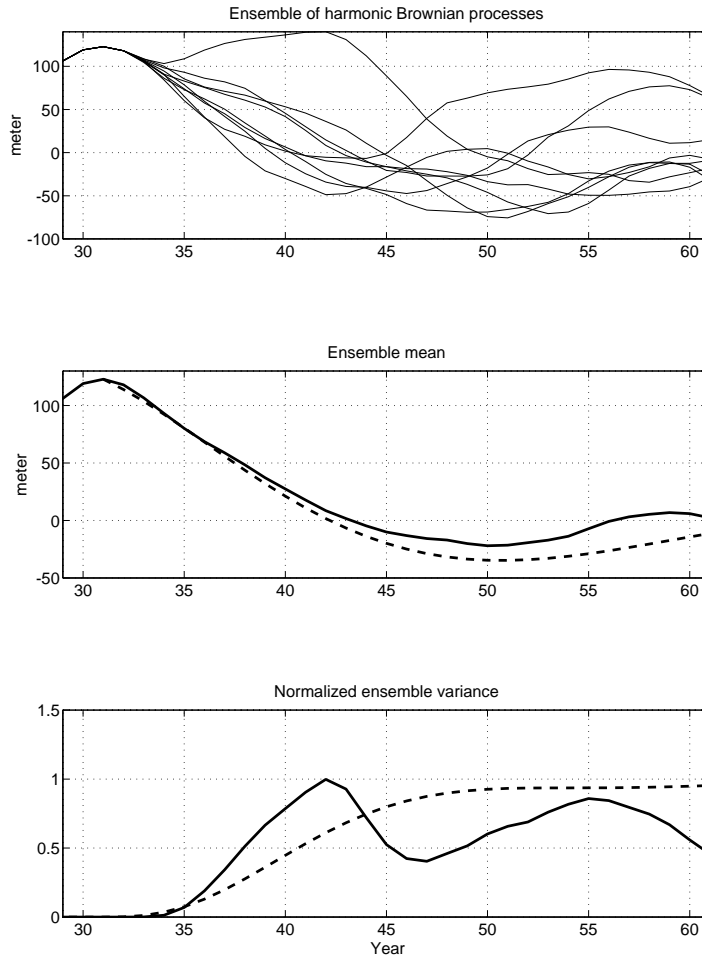


Figure 8: **(A)** A nine element ensemble of the harmonic Brownian process. Each element was integrated for an initial period using the same white noise forcing. Afterwards, the noise is unique to each element. **(B)** The ensemble mean (solid) and the damped harmonic persistence forecast (equation (8); dashed line). **(C)** The ensemble variance (solid) and the error function of the damped harmonic persistence forecast (equation (9); dashed line). The parameters for these forecasts were estimated from the *acf* of Figure 7. Note the approximately zero initial slope in the variance representing the slower initial de-correlation of the ensemble elements relative to the Brownian process ensemble shown in Figure 6.

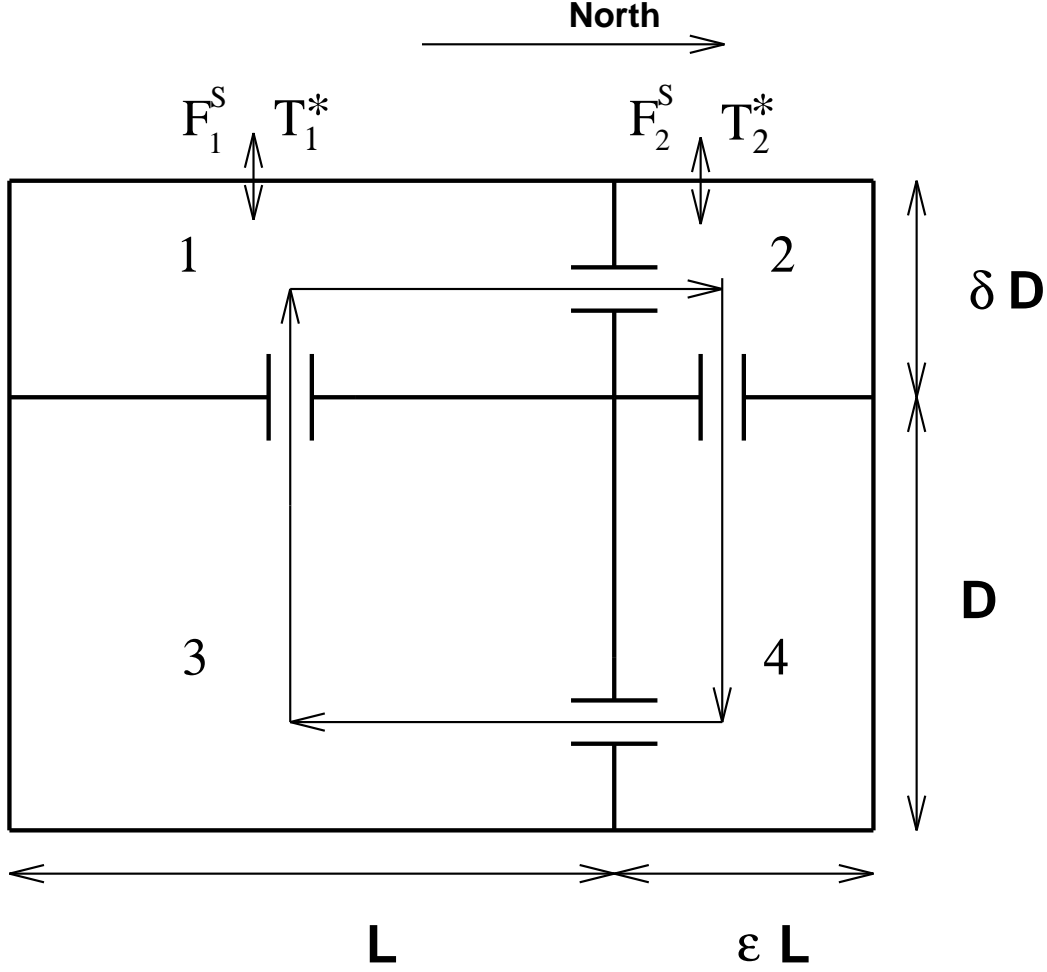


Figure 9: Configuration of the four box model. The thermal driven mean circulation, with sinking in the north and rising in the south, is indicated. The boxes are homogeneous. The parameters chosen for the numerical experiments are the following: $V = 8 \times 10^{16} \text{m}^3$, $\epsilon = .10$, $\delta = .10$, and $D = 3000 \text{m}$. The surface box temperatures are restored to $T_1^* = 25^\circ \text{C}$ and $T_2^* = 0^\circ \text{C}$ with a restoring time $\gamma_T^{-1} = 180$ days, which corresponds to a restoring time of .6 day for each metre depth. The surface salinity forcing $F_{1,2}^S$ is restoring to the salinities $S_1^* = 36.5$ psu and $S_2^* = 34.5$ psu using $\gamma_S = .2\gamma_T$ ($\gamma_S^{-1} = 900$ days) during the integration to steady state. Afterwards, a fixed salinity flux $F_2^S = -\epsilon F_1^S = \gamma_S(S_2^* - \bar{S}_2) < 0$ is used for the mixed boundary condition integrations. Note the four boxes all have different volumes.

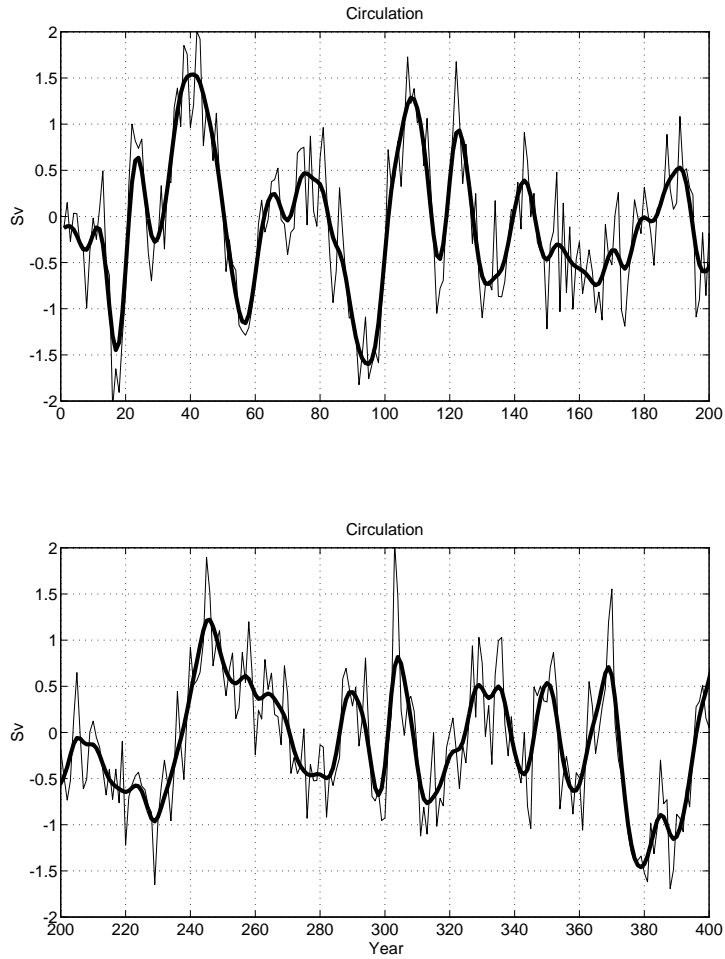


Figure 10: A 400 year realization of the yearly averaged circulation in the four box model (thin solid line). The mean (which has been subtracted) is 19.6 Sv and the standard deviation is .76 Sv. A 10 year low pass filtered (thick solid line) version is also shown. The standard deviation of the filtered time series is .65 Sv. The variability seen in this time series is meant to roughly correspond to that of the THC index generated by the coupled model seen in Figure 1.

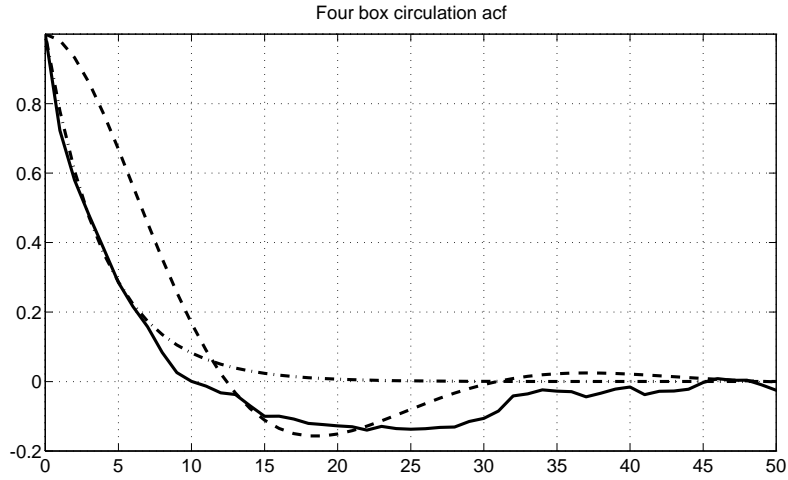


Figure 11: **(A)** *Acf* of the circulation shown in Figure 10. The damped exponential (dot-dashed line) is the *acf* for a Brownian process with e-folding time 4 years. This *acf* matches that of the box model at small lag times reflecting the small time scale exponentially damped modes causing de-correlation at this scale. The damped oscillatory function (dashed line), which matches the *acf* at longer lag times where there is a trough due to the oscillatory eigenmode, is the *acf* for a harmonic Brownian process. The period and decay times of this process are 32 and 10 years, respectively. A similar fit to the low pass climatology (not shown) gives an e-folding of 6 years for the Brownian process and a period and e-folding time of 35 and 12 years, respectively for the harmonic Brownian process. Compare to the *acf* for the coupled model's THC index shown in Figure 2.

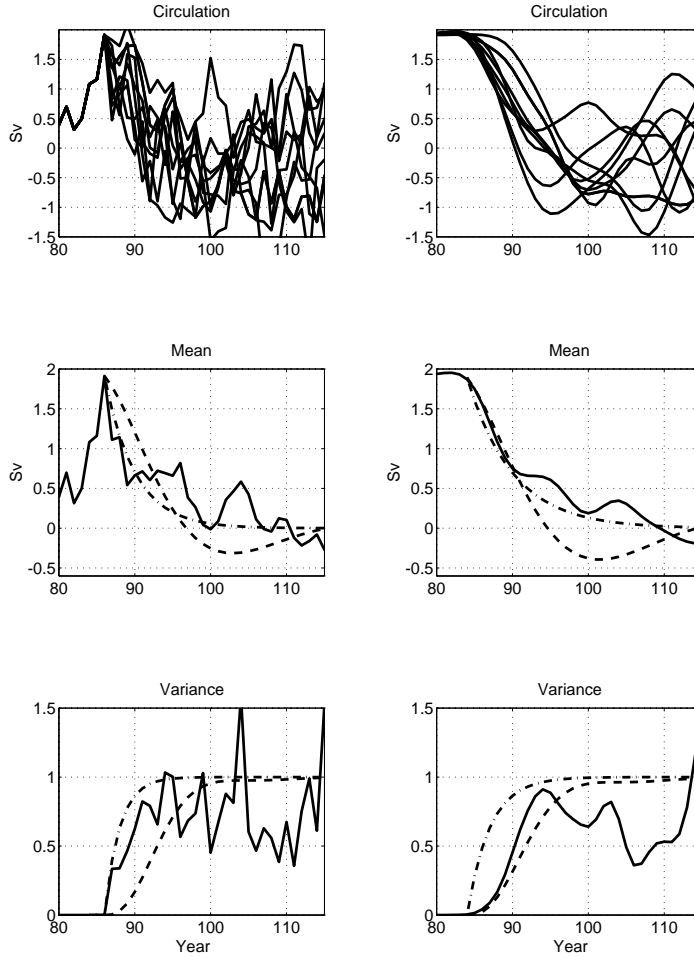


Figure 12: **(A)** A nine element ensemble of yearly averaged circulation from the four box model. **(B)** Ensemble mean(solid line) as well as the mean from an infinite ensemble of Brownian processes (i.e., the damped persistence forecast (2); dot-dashed line) and the mean from an infinite ensemble of harmonic Brownian processes (i.e., the damped harmonic persistence forecast (2); dashed line) using parameters estimated from fits to the climatology in Figure 11. **(C)** Ensemble variance (solid line). Also shown are the variances from the ensemble of Brownian processes (i.e., the error functions from the damped persistence forecast (4); dot-dashed line) and that from the ensemble of harmonic Brownian processes (i.e, the damped harmonic persistence forecast error (9); dashed line). Note the rapid initial growth (slope $\neq 0$) in variance corresponding to the damped persistence forecast. **(D)**, **(E)**, **(F)** are the same as **(A)**, **(B)**, **(C)** after a 10 year low pass filtering is applied. The initial point is extended 10 years prior to the ensemble's start to facilitate low pass filtering. The slower growth in initial ensemble variance resulting from the filtering bringing it somewhat more in line with the variance from the harmonic Brownian process.

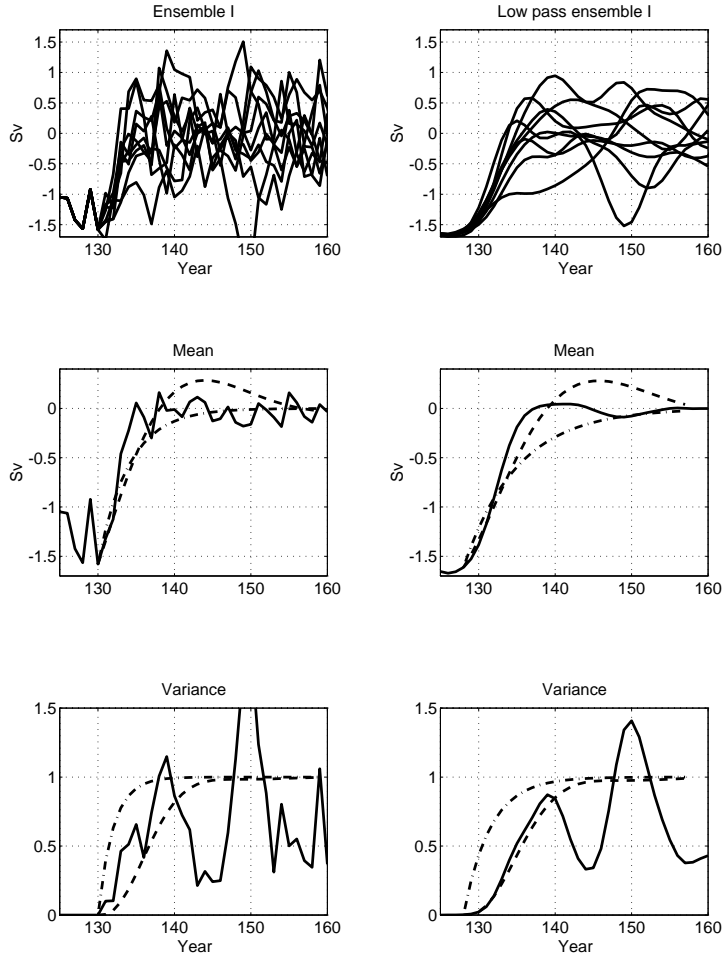


Figure 13: (A) Nine element ensemble of yearly averaged anomalous THC index from the coupled model. The ensemble starts at year 130 and extends for 30 years. (B) The ensemble mean. Also shown are the damped persistence forecasts (dot-dashed) and damped harmonic persistence forecasts (dashed) derived from the fit of the Brownian and harmonic Brownian processes to the 400 year climatology of Figure 2. (C) The normalized ensemble variance. (D) Same as (A) for the 10 year low pass signals where the anomalies are defined relative to the climatology indicated in the caption of Figure 1. (E) Same as (B) for the low pass ensemble. (F) Same as (C) for the low pass ensemble.

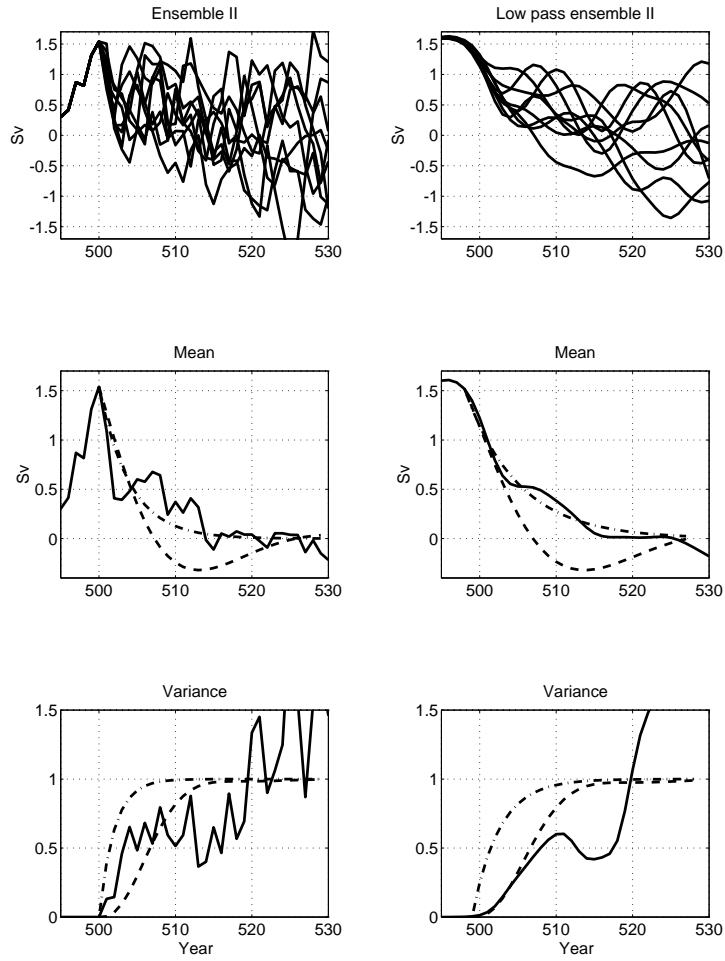


Figure 14: (A)–(F). Same as Figure 13 (A)–(F) for the second coupled model ensemble experiment.